Machine Learning-enabled Optimization of Melt Electro-Writing 3D Printing

Ahmed Choukri Abdullah[1*], Olgac Ozarslan[2*], Sara Soltanabadi Farshi[2], Sajjad Rahmani Dabbagh[1], and Savas Tasoglu[1,3,4,5,6,7,¥]

[1]Department of Mechanical Engineering, Koç University, Sariyer, Istanbul, Turkiye 34450.
[2]Department of Biomedical Sciences and Engineering, Koç University, Sariyer, Istanbul, Turkiye 34450.
[3]Koç University Arçelik Research Center for Creative Industries (KUAR), Koç University, Sariyer, Istanbul, Turkiye 34450.
[4]Koc University Is Bank Artificial Intelligence Lab (KUIS AILab), Koç University, Sariyer, Istanbul 34450, Turkiye.
[5]Koç University Translational Medicine Research Center (KUTTAM), Koç University, Istanbul, Turkey 34450.
[6]Boğaziçi Institute of Biomedical Engineering, Boğaziçi University, Çengelköy, Istanbul, Turkiye 34684.
[7]Physical Intelligence Department, Max Planck Institute for Intelligent Systems, Stuttgart, Germany 70569.
[¥]Corresponding Author: Savas Tasoglu (stasoglu@is.mpg.de).
*These authors equally contributed to the manuscript

Abstract:

Melt electrowriting (MEW) is a solvent-free (i.e., no volatile chemicals), high-resolution 3D printing method that enables the fabrication of semi-flexible structures with rigid polymers. Despite its advantages, the MEW process is sensitive to changes in printing parameters (e.g., voltage, printing pressure, and temperature), which can cause fluid column breakage, jet lag, and/or fiber pulsing, ultimately deteriorating the resolution and printing quality. In spite of the commonly used error-and-trial method to determine the most suitable parameters, here, we present a machine learning (ML)-enabled image analysis-based method for determining the optimum MEW printing parameters through an easy-to-use graphical user interface (GUI). We trained 5 different ML algorithms using 168 MEW 3D print samples, among which the gaussian process regression ML model yielded 93% accuracy of the variability in the dependent variable, 0.12329 on root mean square error for the validation set and 0.015201 mean square error in predicting line thickness. Integration of ML with control feedback loop and MEW can reduce the error-and-trial steps prior to the 3D printing process, decreasing the printing time (i.e., increasing the overall throughput of MEW) and material waste (i.e., improving the cost-effectiveness of MEW). Moreover, embedding trained ML model with the feedback control system in a GUI facilitates a more straightforward use of ML-based optimization techniques in the industrial section (i.e., for users with no ML skills).

Keywords: Melt Electrowriting; additive manufacturing; 3D printing; optimization; image analysis; machine learning; polymer; feedback control

Introduction

Since Hull's invention of the stereolithography (SLA) technology and the construction of the first three-dimensional (3D) printed object in the 1980s, 3D printing has become widely used in a variety of fields, including engineering, manufacturing, medicine, and education [1]. Such small fiber diameters can be facilitated with electrohydrodynamic (EHD) techniques such as melt electrowriting (MEW) and melt electrospinning (MES) [2, 3]. Since its introduction in 2011 [4-6], the MEW has been notably adopted in biomedical applications. The MES, specifically in tissue engineering, is widely preferred due to its non-woven fiber diameters for the application of scaffolds where high porosity is desired [2, 7]. On the other hand, the MEW defines a well-ordered fiber structures and patterns to achieve strong, durable, and organized high porosity scaffold [5] with small fiber diameters [5, 8]. MEW's precision has been embedded in the fabrication of microchannel systems [5, 9] and microfluidics [8] overcoming the conventional techniques [9]. Its application extends across many sectors from optics to photonics and lap-on-chip devices [5, 8]. The accuracy of having such high craft precision for microscale application is due to its control over jetting process and stability [10]. Many parameters influence this stability such as applied pressure, electric field, and collector speed, understanding their interdependence and relation is an area of interest [10]

A MEW device consists of a printing head with a heating system that melts the material stored in a syringe and delivers it to a metal nozzle. A computer-aided translation system is installed in the MEW head, allowing for direct writing onto a collector. The extrusion of the material melt through the nozzle is forced by a delivery system (typically air pressure), and an applied potential difference between the nozzle and the collector generates an electrical field. When an electric field is applied to a fluid drop, it concentrates charges at the closest point to the collector, overcoming surface tension forces and ejecting a conical-shaped jet toward the collector. The beginning of this jet and the remaining fluid at the tip of the nozzle is termed the *Taylor cone* which will be generated within seconds, as soon as the applied electrical field overcomes the surface tension of the droplet at the tip of the nozzle [11]. As the Taylor cone is filled with more molten polymer, the weight of the melt begins to neck from the initial droplet, forming a thin column. This proceeds until the forces (gravitational and charges) draw the solidified polymer to be in contact with the collector. The resulting fiber diameter can be controlled, adjusted, and direct-written in varying configurations depending on the printing parameters [12]. Small-diameter fiber placement enables for the printing of porous structures known as scaffolds, which are used in the biomedical sciences [13]. To date, melt-electrowritten scaffolds have been investigated in the skin, heart valves, and musculoskeletal soft tissues, where poly-ε-caprolactone (PCL) is commonly used [14]. PCL, a Food and Drug Administration-approved bioresorbable polymer, is the biomaterial of choice for constructing tissue-engineered melt electrowritten scaffolds due to its easy processability, low cost, and lack of immunogenicity [15]. Alternatively, when MEW is performed at collector speeds lower than the electrified jet speed, the jet buckles, similar to a column of honey falling onto toast [16]. Such mechanical

buckling of a viscoelastic column produces an array of different patterns that can be modeled and predicted [17].

In this paper, we introduce an innovative methodology for combining the fields of MEW, image processing, ML and control theory to be embedded within a friendly GUI. First, samples from the MEW at different setup of printing parameters has been printed and collected. 4 input parameters were used for this purpose; the pressure at which air is compressed into the MEW's nozzle, the speed at which the feed rate of material is extruded, the gap between the nozzle and printing surface, and high voltage difference between applied between the nozzle and print bed. Second, a custom-designed algorithm image processing technique carried out for line thickness calculation. Upon the collection of data, some prints are classified as "bad prints" as these patterns are not preferred in the real printing process. Only "good prints" were undertaken in the image processing part. Third, the dataset collected were preprocessed and trained in ML regression models where a Bayesian hyperparameter optimization has been handled. Fourth, a PID controllers for each of the four inputs are tuned according to the sensitivities returns of the plant (regression) model. A saturation and anti-windup configuration within the controllers were used. Finally, a GUI has been developed that provides a user-friendly interface to grant instant feedback and to enhance the user experience and visual representation.

Methods

Device: The MEW bio-printer used for this study was manufactured by Axolotl Biosystems in Istanbul, Turkey. The Axolotl printer comes with multi-head components for where it offers versatile usage, enabling users to switch between different printing materials, methods, or applications via swapping the printheads upon the desired request of the user. The specific printer from Axolotl is equipped with a UV curing toolhead that facilitates the photocrosslinking of biomaterials and bioinks, a high/low temperature printheads that demands a high/low temperature extrusion of several polymer types for working with bioresorbable and biocompatible materials, and a MEW printhead. The MEW printhead can simultaneously deposit multiple layers allowing for intricate design and the integration of functionalities within a single print session. It also capable of writing melted material with high voltage, hence the name "Melt ElectroWriting". The Axo MEW can achieve micro-level of precision that provides a 3D fabrication of fiber scaffolds which aids in the various medical applications such as tissue engineering and regenerative medicine. The printer was specifically set to electrowrite line thickness for voltages that fall in ranges of 2 to 3 kV, gaps of 0.2 to 1 mm, pressures of 1 to 23 psi, printhead's feedrate of 300 to 2000 mm/min, and a stable printhead temperature of 150 °C.

Material: The printing material used in this study was Polycaprolactone (PCL). PCL is a dielectric material, which means it is an insulator that can become polarized when subjected to an electric field [18]. When an electric field is applied to PCL, the positive and negative charges within the polymer molecules may shift and align themselves with the field direction. This phenomenon is known as polarization. Therefore, PCL is a suitable material for the MEW 3D printer that uses electric field difference (EFD) between the nozzle and the

print surface to ensure a steady flow of the material out of the nozzle by overcoming the surface tension of the molten polymer, causing it to elongate and form a continuous filament or jet [3].

Line thickness experiments: The line thickness of printed designs is of great importance as it can determine the print resolution and mechanical properties. In microfluidic applications, in which MEW is used for the fabrication of negative mold [19], line thickness control is necessary to obtain the designed channel width/thickness. Decisive paraments affecting the line thickness can be cartridge temperature, print pressure, EFD between the nozzle and the printing surface, printing gap, and print speed (i.e., feed rate). The study aims to develop an ML-enabled platform through which a user can find the best combination of printing parameters (e.g., print pressure and voltage) to acquire desired line thickness without a need for error-and-trial steps, resulting in a faster process time and less material waste (Figure 1).

Printing and Imaging: Firstly, using SolidWorks software, nine similar straight lines (with the same thickness of 0.2 mm) (Figure 2E) were drawn and exported to the 3D printer as G-code. The thickness of lines was set to be the same in the CAD design to minimize the effect of design and focus/study the pure effect of print parameters on the thickness of the designed lines. Next, each of line was printed using a different combination of printing parameters (Figure 2F). For example, for the first set of nice lines, to study the effects of printing pressure on the line thickness, all the abovementioned printing parameters were kept constant, while the printing pressure was changed at the beginning of each line. Upon completion of the printing process, the printed design was removed from the printer to capture images of the printed lines using a microscope. All images were taken from the same lens distance to maintain a similar aspect ratio in all images. Captured images were then labeled with the printing parameters used for the 3D printing of the line in the image and fed into a custom-designed image processing algorithm for the automatic calculation of line thickness. The same process was repeated for other printing parameters (e.g., printing with different EFD while other abovementioned parameters were kept constant). The cartridge temperature was set to 150 °C during all experiments, as per the guideline of the Axolotl company.

Custom-designed algorithm for line thickness calculation: We developed an image processing method which can automatically calculate the thickness of the line in a captured image. In the context of image processing, our developed algorithm plays a pivotal role in automatically quantifying line thickness from captured images. Commencing with the conversion of images to grayscale, it subsequently applies Gaussian blur to mitigate noise while retaining line continuity. Employing thresholding, it transforms the image into binary format, distinguishing line pixels from the background. Significantly, our method utilizes a 3x3 filter to effectively eliminate isolated black pixels, minimizing potential outliers. By systematically evaluating each column, the algorithm counts consecutive black pixels to determine line thickness. This culminates in the computation of an average thickness value. The resulting data, including image names, printing parameters (pressure, gap, EFD), feed rate, and line thickness, are methodically stored in a CSV file. This comprehensive approach

not only facilitates the precise measurement of line thickness but also enhances the utility of this data for machine learning training and GUI development in a variety of applications. Figure 2 illustrates the process where each step of the image processing method is detailed.

Machine Learning: Machine learning (ML) is a subset of artificial intelligence (AI) that focuses on the design of systems so that they can learn and make predictions based on previous experience that is called data [20]. The algorithm should first be trained on the data in the training set in which the parameters in the algorithm will be improved during the training process, and a machine learning model will be generated. It can then predict the results with new input data using the updated machine learning parameters. Supervised learning, unsupervised learning, and reinforcement learning are the most often used machine learning algorithms [20].

An ML model was developed to correlate the printer's input parameters and line thickness retrieved previously by the custom-designed algorithm for line thickness calculation. Regression models were employed to map 4 printer's parameters and the single output line thickness captured by the algorithm. To ensure faster convergence, enhance the accuracy of ML models, and prevent numerical instabilities, the input dataset was normalized to a consistent scale ranging from [-1 1], while the output data remained unchanged. Out of a total of 168 printed samples, the dataset was divided into training and validation sets using an 80:20 ratio, where only 34 datapoints were reserved for validation after model training. Different ML models such as linear, vector support machine (SVM), decision trees, gaussian process (GP), neural network (NN) along with other regressions were trained with the remaining dataset. The models were assessed based on their mean squared error (MSE), root MSE (RMSE) and R^2 scores, with the aim of minimizing potential errors during both computation and execution phases.

To optimize the performance of the various ML models, they were subjected to Bayesian optimizer for tuning the hyperparameter optimization. Unlike grid search or random search methods which either exhaustively explore or randomly sample the hyperparameter space, the Bayesian optimizer uses an intensive search across the hyperparameter space which constructs a probabilistic model of function that maps hyperparameters with a given validation score allowing it to thoroughly explore the hyperparameter space. It then can create an approximation of the error as a function of the hyperparameters to improve the model. The learning process was set for 30 iterations which updates the model based on observed performances, hence, Bayesian optimization can more efficiently locate optimal hyperparameter configurations. Therefore, the hyperparameters were tweaked for each ML models to ensure that our models were configured in an optimal manner. Thus, enhancing their performance on the validation set. Again, model performance was evaluated based on MSE, RMSE and R^2 scores.

Sensitivity and Feedback Control: Seeking to attain the results of the line thickness from our previously obtained regression model, it serves as the core plant model in the controller feedback loop. Due to the shortage availability in dataset, this controller design approach solves the related issue. The proposed approach is mentioned as shown in Figure

1. Each of the four inputs was controlled and managed by four PID controllers that minimizes the error coming from the feedback loop. The main drawback of this method is to be able to tune all the four PID controllers, hence, 12 parameters of P, I, and D combined. Despite that the tedious and complicated job, tuning those parameters was guided with the help of *PIDTuner* and *Sensitivity Analyzer* apps within MATLAB and Simulink environment.

The target system behavior in the multi-input single-output (MISO) system was determined by a reference setpoint of a desired line thickness. In a feedback loop, the actual output from the plant model is subtracted from the reference point and fed into the controllers. The controllers then attempt to settle, manage, and adjust the deviation between plant's prediction and reference setpoint by correcting new inputs values relayed back into the system. The loop correction is maintained as it ensures the system continually adjusts its behavior, aligning with the reference setpoint over time.

PID stands for Proportional, Integral, Derivative which are the three types of control "actions". The Proportional term amplifies the error value by a proportional gain. It is essentially the response to the present error in the model. The Integral term is responsible for all summation of past error values accumulated by the model. Inherently, the integral term attempts to eliminate and drive the system to zero steady state error by an integral gain. Finally, the Derivative term anticipates the system response based on its rate of change in error. The derivative gain control the effect of future error, thus, slowing down the rate of change in error. Each of the input parameters exhibits its own influence on the line thickness output in the plant model. The pressure and speed have the most impact on the model compared to the voltage and gap parameters. Therefore, a tuning in PID parameters was accompanied by a sensitivity analysis to assess the behavior of each input on the system. Whether one parameter is more sensitive to changes from another or more robust, etc. Additionally, the PID controllers where saturated at limits of [-1 1] in agreement with the regression model obtained earlier.

Results and Discussion

1. Results ML

Several machine learning models are trained. Yet, we only picked the one which outperformed the other models in terms of RMSE, MSE, and R^2 scores. The validated scores of the regression models fall between 0.12, 0.015, 0.93 and 0.15, 0.024, 0.89 of RMSE, MSE and R^2, respectively. The MSE is the average of the squared error difference between the predicted and actual values that measures the average magnitude of the error, while the RMSE is simply the square root of the MSE which provides interpretable readings of the error magnitudes since it's in the same unit at the output. The lower of these errors the better the model's performance. The R^2, also known as the coefficient of determination, provides a measure of how well the observed outcomes are being replicated by the model. It ranges from 0 to 1 (1 for a perfect score). These results were recorded when a Bayesian hyperparameter optimizer utilized. The GP regression was our best model for this work

which optimized 5 hyperparameters namely: basis function, kernel function, kernel scale, sigma, and whether standardize is on or off. The search ranges of each hyperparameter were predefined automatically. For example, the basis function could be a constant, a zero, or a linear function; the kernel function can be nonisotropic exponential, nonisotropic rational quadratic, isotropic ration quadratic, etc. For each set of ranges, the Bayesian optimizer ran for 30 iterations looking for the best outcome using the several combinations of hyperparameters within the ranges. Additionally, the acquisition function in the Bayesian optimizer was set to expected improvement per second which takes into consideration the improvement in objection function and time required to evaluate the function. Finally, the optimized hyperparameters were found according to the selected search criteria and the training results were provided. As previously mentioned, the GP regression surpassed the performance of all other regression algorithms. This can be attributed to its ability to accurately model intricate data in non-parametric models. Moreover, GP regression effectively filters and manages noise inherent in the dataset along with uncertainties arising during training. We observed the following results for our GP regression model: the RMSE, MSE, R^2 were recorded at 0.12329, 0.015201, and 0.93, respectively. Figure 4A provides an insight of the GP regression model obtained for perfect prediction and imposed datapoints in normalized range. The hyperparameters that were calculated by the Bayesian optimizer are supported in Table 1. A RMSE of 0.12329 indicates that there is a deviation in predicted line thickness by this amount. Due to the nature of the dataset, taking the average between the minimum and maximum line thickness that are within the dataset (0.0172 and 2.2635, respectively) results in around 10.8% error. This has been also proven by the remaining 34 datapoints in the testing set yielded 0.1054 for RMSE score. The discrepancy in scores can be explained by the limited number of prints in our experimental as it was tedious to print all these prints. Yet, a ten percent error can be accepted in our work due to the absence of other negligible factors.

2. Results of Sensitivity and Feedback Control

In the line of sensitivity results, the PID controllers were tuned separately and observed their impact on the output model. The sensitivity chart shows that pressure and speed had the most influence over the model as providing typically a lower Proportional gain to the parameters compared to the gap and voltage, Figure 4B. On the other hand, the gap and voltage need a high Proportional value to avoid slow response and reach the setpoint quickly. Yet, a higher Proportional gain could lead to overshoot to the system. Thus, balancing between the Proportional gain among the input parameters is required. The sensitivity analysis also provides an insight after tuning the Proportional gain whether the inputs are oscillating around the setpoint or not reaching the desired output. The integral gain is introduced into the system to eliminate long term steady-state error. A Derivative term was needed to speed up the system's response but could also introduce overshoots and noises to the system. Again, refining the gains based on the sensitivity chart to balance between robustness and aggressiveness in the regression model was an important step in the controller design phase. Interestingly, the sensitivity chart also provided the sign correlation between the input parameter and its output. Pressure has a negative correlation with the line thickness which indicates an inverse relationship, e.g., thinner line thickness in response to increasing pressure value. Whereas the speed has a direct affect as computed.

After successive tuning each PID controller individually, the controllers struggle to bring the MISO system to the desired setpoint. This was due to nonlinearities within the controllers when they were saturated in [-1 1] ranges. Therefore, an anti-windup strategy through back-calculation within each controller was implemented. The anti-windup technique avoids the accumulation of error within the controller when its output exceeds the saturation limits [21-23]. This could cause overshoot, prolong settling times, and "stuck" behavior. The anti-windup mechanism is built in the Integral gain that acts as a break whenever the saturation limits at the output is reached. The back-calculation anti-windup takes the difference between the saturated value and the actual PID output is fed back to the integrator to subtract it from the accumulated error in the feedback loop [23]. Moreover, the back-calculation coefficient determines how aggressively the accumulated integral error is to be adjusted when the saturation occurs [24, 25]. Finally, the controller designs, incorporating the anti-windup mechanism for output saturation, were correctly tuned using untrained dataset in alignment with the provided sensitivity analysis. Figure 4C visualized the schematic control diagram along with associated PID gains in Table 2.

3. Graphical User Interface (GUI)

A GUI of the line thickness model has been integrated within the feedback controller discussed earlier. Our primary objective is to be able to validate and operate the line thickness model where non-experienced users can utilize it. With this easy-to-use interface, users can easily monitor on *running* status, to know the model is at the running mode, and patiently wait for the operation to end (*evaluation finished*) without the need of manual interruption. The GUI allows users to enter the desired line thickness, denying negative numbers. Upon activating the *calculate* button, the system initializes the Simulink model at the background where it tries to track the error arising from the feedback loop of the controllers. Then finally displaying the printer's input parameters within the interface. Additionally, the GUI can't execute another calculation while it's on the *running* status as shown in Figure 5.

4. Validation

The validation step of our work was of highly importance as the development of the final product, GUI of line thickness. We prepared a list of some desired line thickness to be fabricated by the MEW. The previous lines which were printed and collected as training dataset, were specified through CAD drawings, keeping the temperature, feed rate, voltage, and gap constant and while altering the pressure values to produce the dataset. However, this time, we specified the four input parameters to the printer configuration that has been predetermined by the GUI. The expected results were to show some error deviation from the actual thickness, as provided from ML model. Yet, after postprocessing the new validated results, the observed line thickness from the custom algorithm layout a line thick that is on average two times wider than the desired line thickness (Table 3). This claim can be explained via the error made in the regression model and the controllers' approximation on PID values. On the other side, the MEW printer's settings have been modified from the dataset collection due to technical issues with the printing heads. We have accounted for the ratio between the desired and obtained line thickness from the algorithm by defining an

error factor constant, ranging between 2.2-2.4, to isolate and narrow down the difference. By addressing the mismatch, we were able to recreate new line thicknesses to matched down our desired prediction from GUI with acceptable difference of 5-7% error after adding the error factor.

Conclusion

In conclusion, this study provides an insight of how a MEW printer can be implemented with ML along with feedback controllers in which it can be designed and build inside a GUI for friendly use. Around 160 prints from the MEW printer were used to train different ML algorithms and based on certain criteria, the best regression model was used to represent the *plant* model in our feedback loop in the controller phase design. The prints were captured through microscope and reported their input printer's parameters where each datapoint had unique inputs during the data extraction. Then image classification and image processing techniques were imposed to filter and classify "good" and "bad" prints that resulted in fabrication. Upon disregarding the "bad" prints, the classified "good" prints were filtered into a custom-designed algorithm to calculate the line thickness approximation. The collected results of line thickness along with the printer's input parameters made up the dataset that was trained in regression analysis where GP regression provided the best performance with 0.12329 RMSE, 0.015201 MSE, and 0.93 R^2 scores. Moreover, to link between the desired line thickness and printer's input parameters, the model line thickness was implemented as a *plant* in a feedback controller loop where it returns the original model prediction from GP regression and reduces the error between the desired line thickness and model prediction from GP regression through the PID controllers. Additionally, the controllers were tuned according to the sensitivity of the input parameters using analyzer apps within the MATLAB environment. Finally, the whole system was customized and compacted to be made possible for a free to access in a GUI where the users would enter the desired line thickness as wishes then at background evaluation, the model would provide the printer's input parameters. The proposed methodology not only enhances the accessibility of the system but also paves the way for broader applications, ensuring that possible further improvements and fixes in model at expertise levels.

Acknowledgment

ST acknowledges Tubitak 2232 International Fellowship for Outstanding Researchers Award (118C391), Alexander von Humboldt Research Fellowship for Experienced Researchers, Marie Skłodowska-Curie Individual Fellowship (101003361), and Royal Academy Newton-Katip Çelebi Transforming Systems Through Partnership Award (120N019) for financial support of this research. Opinions, interpretations, conclusions, and recommendations are those of the author and are not necessarily endorsed by the TÜBİTAK. This work was partially supported by Science Academy's Young Scientist Awards Program (BAGEP), Outstanding Young Scientists Awards (GEBİP), and Bilim Kahramanlari Dernegi The Young

Scientist Award. This study was conducted using the service and infrastructure of Koç University Translational Medicine Research Center (KUTTAM). The authors have no other relevant affiliations or financial involvement with any organization or entity with a financial interest in or financial conflict with the subject matter or materials discussed in the manuscript apart from those disclosed.

References

1. Tetsuka, H. and S.R. Shin, *Materials and technical innovations in 3D printing in biomedical applications.* Journal of Materials Chemistry B, 2020. **8**(15): p. 2930-2950.
2. Brown, T.D., et al., *Melt electrospinning of poly(epsilon-caprolactone) scaffolds: phenomenological observations associated with collection and direct writing.* Mater Sci Eng C Mater Biol Appl, 2014. **45**: p. 698-708.
3. Kade, J.C. and P.D. Dalton, *Polymers for Melt Electrowriting.* Advanced Healthcare Materials, 2021. **10**(1): p. 2001232.
4. Hutmacher, D.W. and P.D. Dalton, *Melt Electrospinning.* Chemistry – An Asian Journal, 2011. **6**(1): p. 44-56.
5. Eichholz, K.F., et al., *How to design, develop and build a fully-integrated melt electrowriting 3D printer.* Additive Manufacturing, 2022. **58**: p. 102998.
6. Brown, T.D., P.D. Dalton, and D.W. Hutmacher, *Direct Writing By Way of Melt Electrospinning.* Advanced Materials, 2011. **23**(47): p. 5651-5657.
7. Hutmacher, D.W., *Scaffold design and fabrication technologies for engineering tissues--state of the art and future perspectives.* J Biomater Sci Polym Ed, 2001. **12**(1): p. 107-24.
8. Dalton, P.D., *Melt electrowriting with additive manufacturing principles.* Current Opinion in Biomedical Engineering, 2017. **2**: p. 49-57.
9. Nadernezhad, A., et al., *Melt Electrowriting of Isomalt for High-Resolution Templating of Embedded Microchannels.* Advanced Materials Technologies, 2021. **6**(8): p. 2100221.
10. O'Neill, K.L. and P.D. Dalton, *A Decade of Melt Electrowriting.* Small Methods, 2023. **7**(7): p. 2201589.
11. Reneker, D.H. and A.L. Yarin, *Electrospinning jets and polymer nanofibers.* Polymer, 2008. **49**(10): p. 2387-2425.
12. Hrynevich, A., et al., *Dimension-Based Design of Melt Electrowritten Scaffolds.* Small, 2018. **14**(22): p. 1800232.
13. Paxton, N.C., et al., *Design tools for patient specific and highly controlled melt electrowritten scaffolds.* Journal of the Mechanical Behavior of Biomedical Materials, 2020. **105**: p. 103695.
14. Castilho, M., et al., *Melt Electrowriting Allows Tailored Microstructural and Mechanical Design of Scaffolds to Advance Functional Human Myocardial Tissue Formation.* Advanced Functional Materials, 2018. **28**(40): p. 1803151.
15. Malikmammadov, E., et al., *PCL and PCL-based materials in biomedical applications.* Journal of Biomaterials science, Polymer edition, 2018. **29**(7-9): p. 863-893.
16. Brun, P.T., et al., *Liquid Ropes: A Geometrical Model for Thin Viscous Jet Instabilities.* Physical Review Letters, 2015. **114**(17): p. 174501.
17. Hochleitner, G., et al., *Melt electrowriting below the critical translation speed to fabricate crimped elastomer scaffolds with non-linear extension behaviour mimicking that of ligaments and tendons.* Acta Biomaterialia, 2018. **72**: p. 110-120.
18. Shahverdi, M., et al., *Melt electrowriting of PLA, PCL, and composite PLA/PCL scaffolds for tissue engineering application.* Sci Rep, 2022. **12**(1): p. 19935.
19. Liu, E.I., et al., *A Versatile Method to Create Perfusable, Capillary-Scale Channels in Cell-Laden Hydrogels Using Melt Electrowriting.* Macromolecular Materials and Engineering, 2023. **308**(9): p. 2300042.
20. Yu, C. and J. Jiang, *A perspective on using machine learning in 3D bioprinting.* International Journal of Bioprinting, 2020. **6**(1).
21. Galeani, S., et al., *A Tutorial on Modern Anti-windup Design.* European Journal of Control, 2009. **15**(3): p. 418-440.
22. Kothare, M.V., et al., *A unified framework for the study of anti-windup designs.* Automatica, 1994. **30**(12): p. 1869-1883.
23. Turner, M.C., J. Sofrony, and E. Prempain, *Anti-windup for model-reference adaptive control schemes with rate-limits.* Systems & Control Letters, 2020. **137**: p. 104630.

24. Murad, M.A.A., M. Liu, and F. Milano, *Modeling and Simulation of Variable Limits on Conditional Anti-Windup PI Controllers for VSC-Based Devices.* IEEE Transactions on Circuits and Systems I: Regular Papers, 2021. **68**(7): p. 3079-3088.
25. da Silva, L.R., R.C.C. Flesch, and J.E. Normey-Rico, *Analysis of Anti-windup Techniques in PID Control of Processes with Measurement Noise∗∗This work was supported by the Brazilian National Council for Scientific and Technological Development (CNPq) under Grants 311024/2015-7 and 305785/2015-0.* IFAC-PapersOnLine, 2018. **51**(4): p. 948-953.

Figures

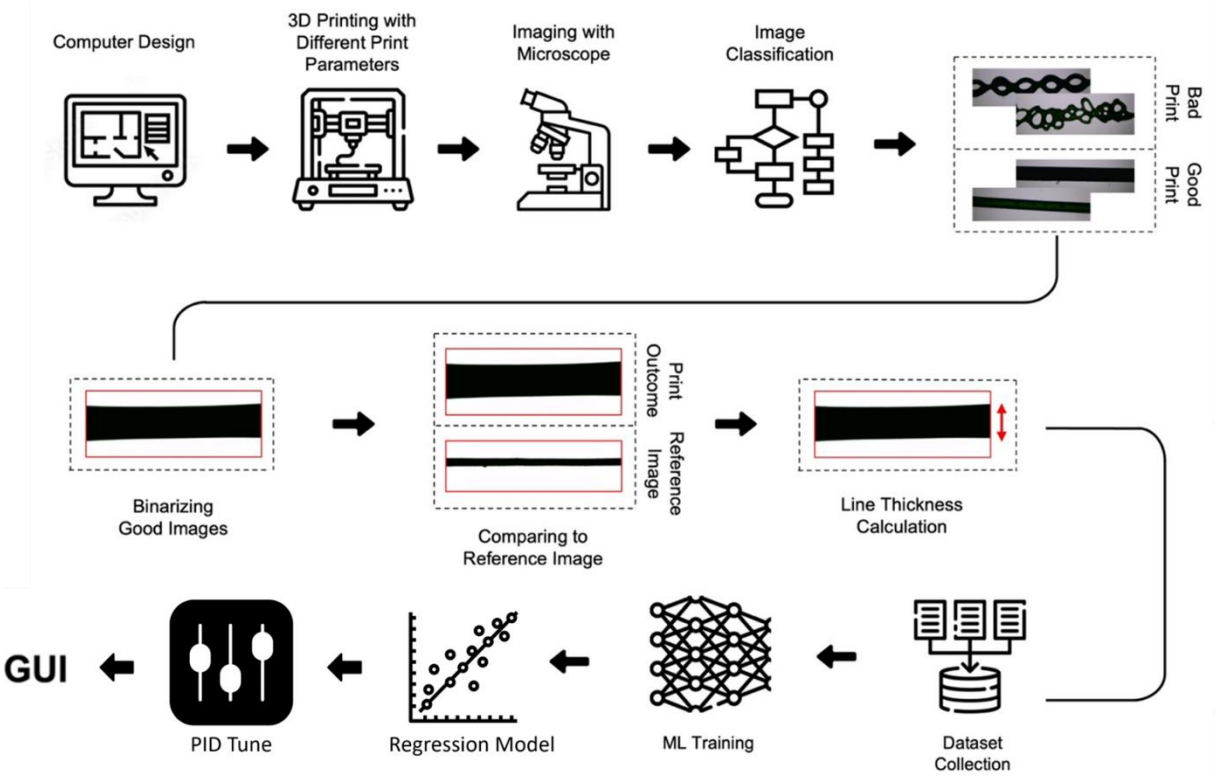

Figure 1. Schematic workflow of "line thickness" calculation and training. Designed patterns were transferred to the MEW 3D printer as G-code, where different printing parameters (e.g., pressure, voltage, etc.) were used to fabricate lines with different thicknesses. Images of the 3D-printed lines were taken under a microscope. A custom-designed algorithm classified straightly printed lines (labeled as "Good Prints") from curvy print outcomes (labeled as "Bad Prints" as these patterns are not preferred in the real printing process). Images with "Good" labels were binarized for better visualization and image processing (i.e., changing pixels to black and white). Next, a standard stencil card was used, on which a standard line with a predetermined thickness of 0.1 mm was drawn. The same microscope and imaging distance were used to capture the image of the standard line. Later, the image of the standard line was used to determine the thickness of the rest of the lines in the captured images. Subsequently, line thickness was collected in a CSV file which was used for ML algorithm training. Next, the trained ML regression model is implemented in a feedback loop using PID controllers where each controller was tuned according to the sensitivity of the model. Finally, the model system can assist MEW users in determining optimum printing parameters to achieve a desired line thickness without the need for error-and-trail steps.

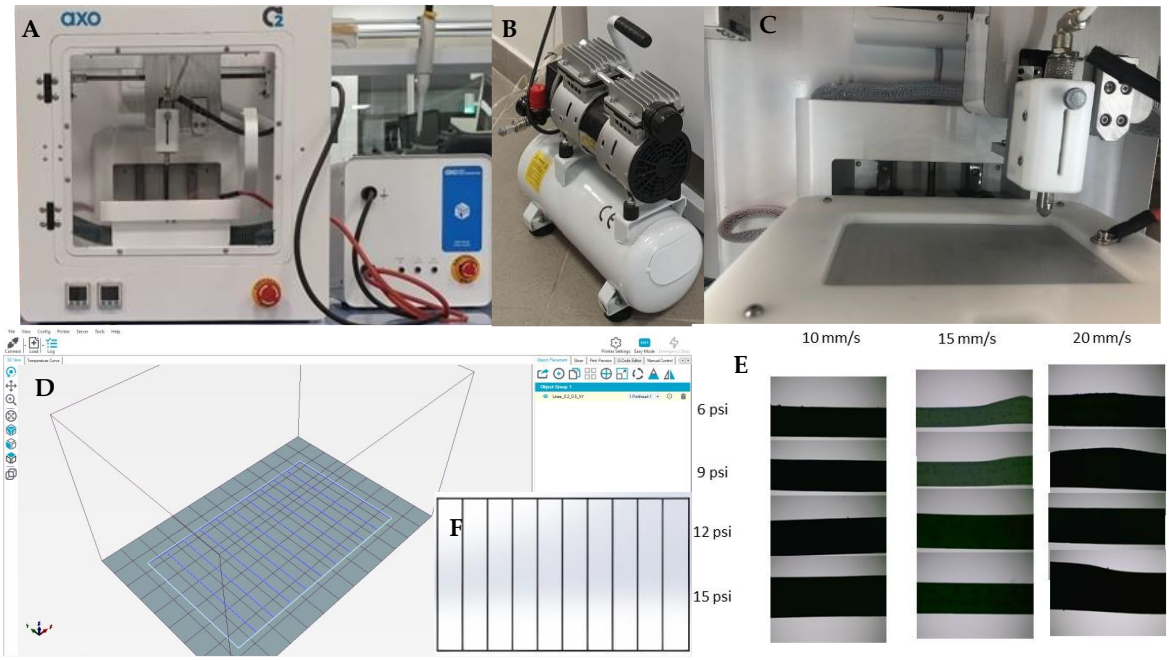

Figure 2: Printer Setup; A) the MEW (shown on top left) along with the voltage supplier. B) The air pressure supplier that pumps air to the nozzle head of MEW. C) The MEW printhead mounted onto the Axo BiosystemPrinter (shown on top right). D) Additionally, the Repetier-host software used as an interface to print the specified loaded CAD files to the MEW printer (shown on bottom right). E) The different combination of air pressure and federate obtained during the experimental printing of the line thickness. F) Similar lines (with the same thickness of 0.2 mm) were drawn in 3D using Solidworks then exported to printer as G-code. each of line was printed using a different combination of printing parameters.

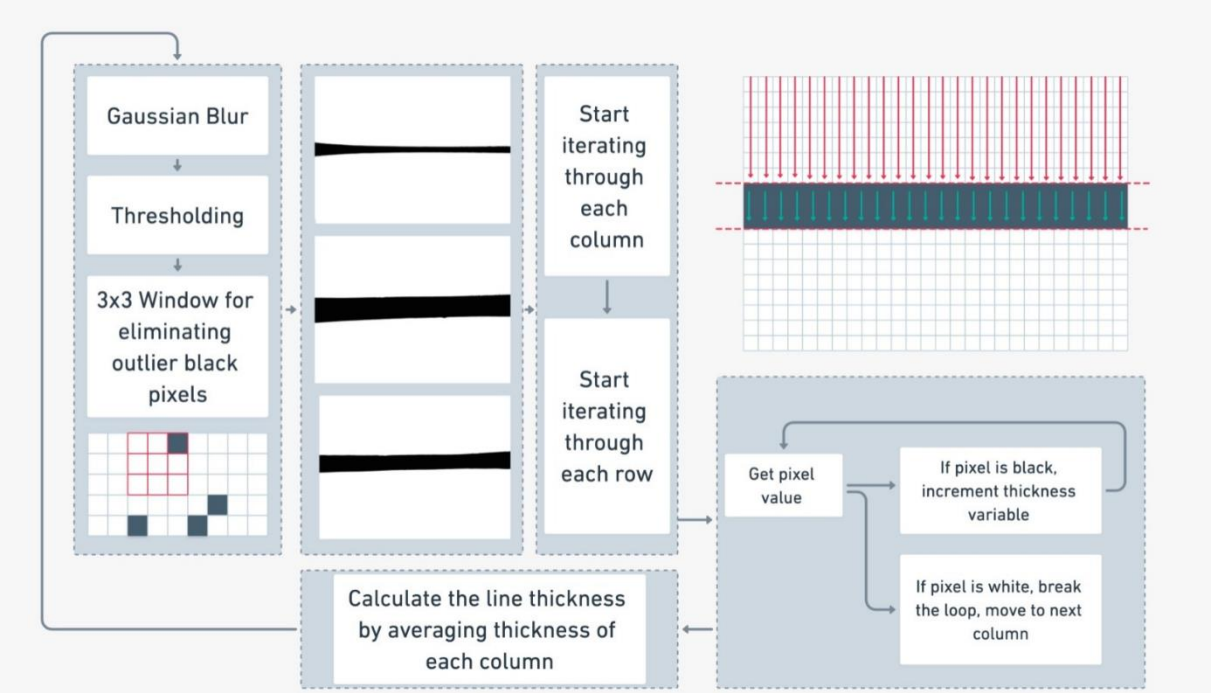

Figure 3: Flowchart of our developed image processing method for automatic line thickness quantification. Beginning with grayscale conversion and Gaussian blur application for noise reduction, the algorithm subsequently employs thresholding and a 3x3 filter to detect and refine the line structure. The method calculates line thickness by counting consecutive black pixels column-wise, resulting in an average thickness value. All data, encompassing image names, printing parameters, feed rate, and line thickness, are archived in a CSV file.

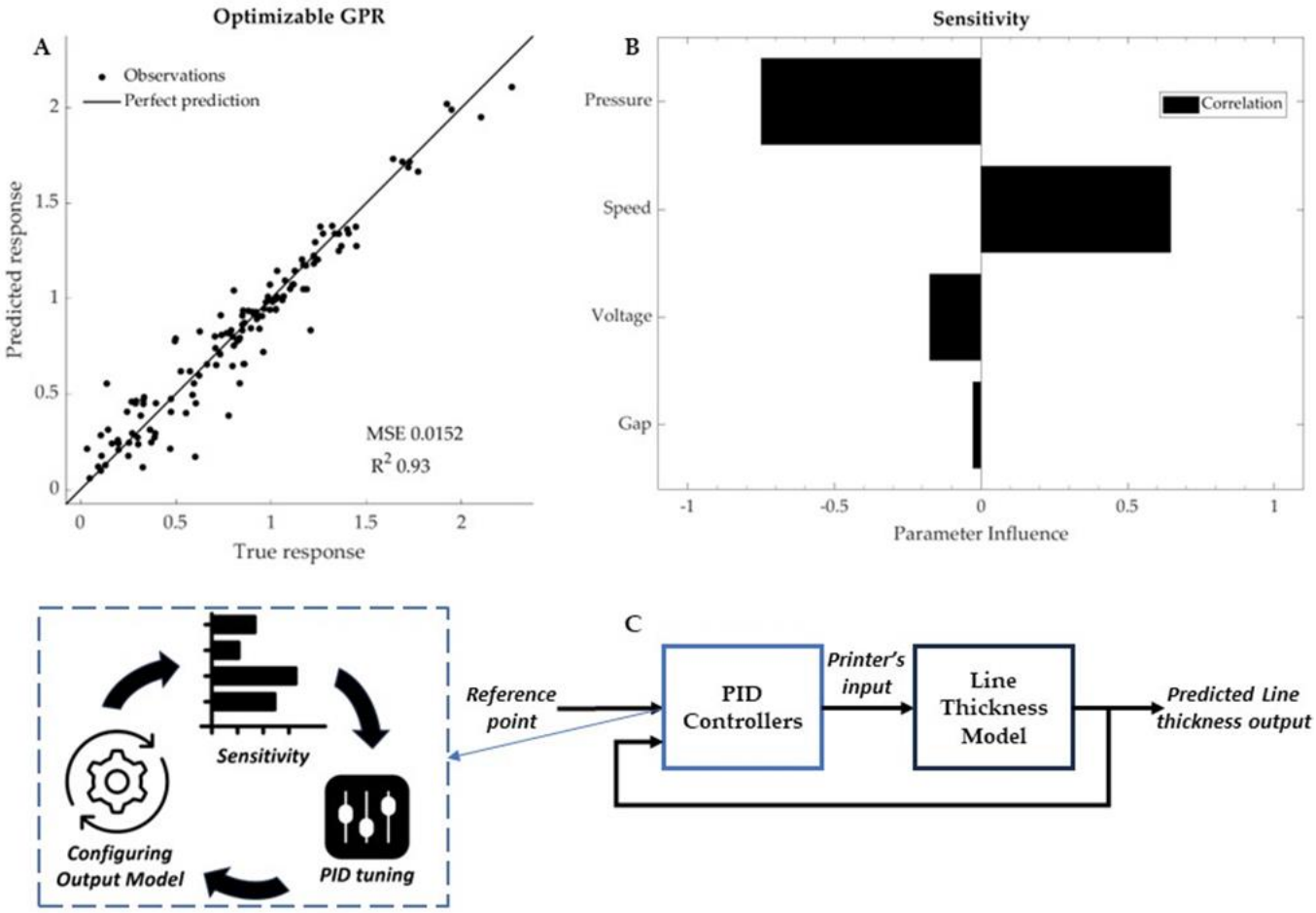

Figure 4: A) The ML regression model obtained for the hyperparametrized GPR with MSE of 0.0152, R2 of 0.93, and RMSE of 0.12. For a normalized perfect model, the true and predicted responses are equal identified by the straight line. The observations of the dataset are shown in black dots. B) The sensitivity analysis of printer's inputs obtained for pressure, speed, voltage, and gap. The pressure and speed have the most impact on the model output, where the pressure has an inverse effect. While the voltage and gap have little effect on the printer's thickness. C) The designed feedback controller loop of the whole analysis. The tuning of 4 PID controllers are accomplished based on the sensitivity chart obtained previously. The input parameters that have most of the influence (e.g, pressure & speed) would have lower Proportional gain relative to the diminished influence (e.g, gap & voltage). Integral and Derivative gains are adjusted based on the behavior and the performance of the model.

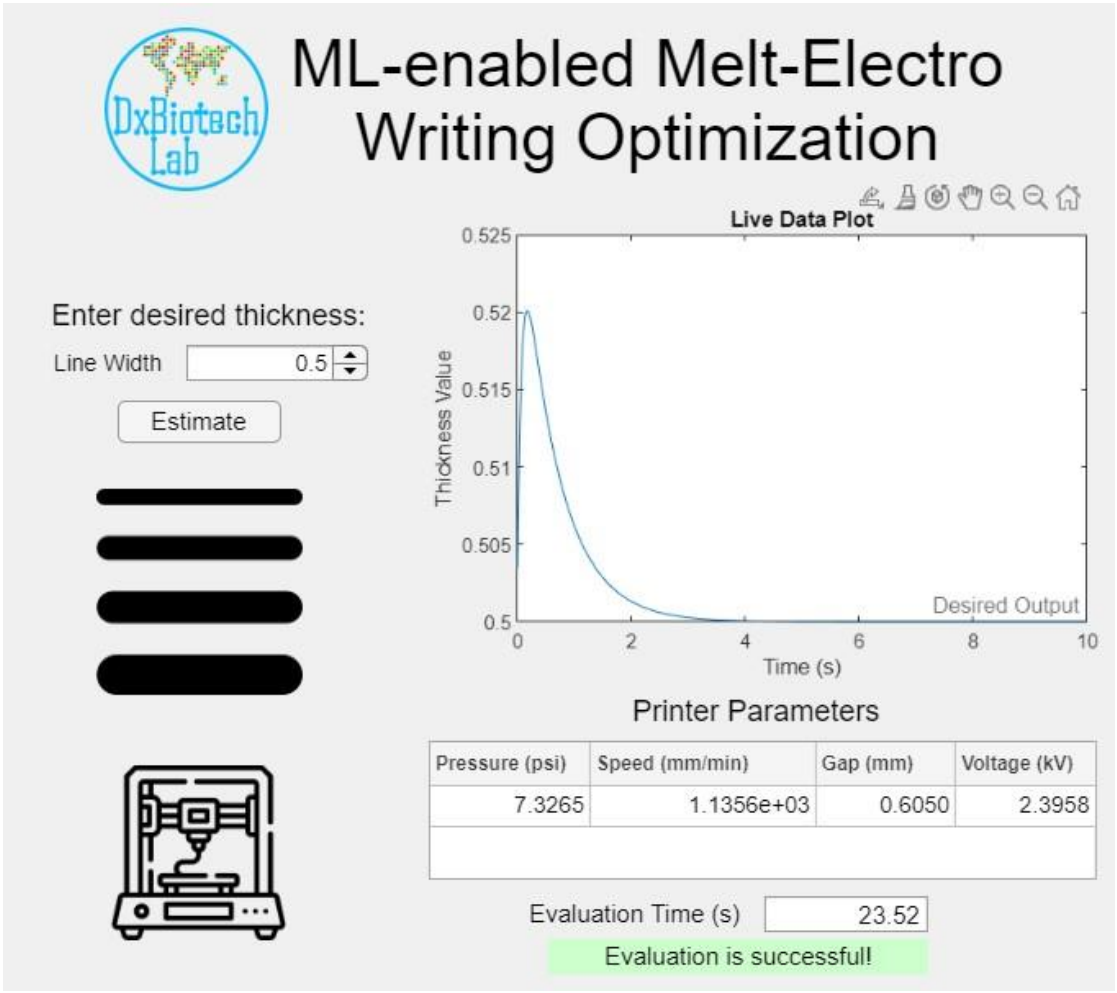

Figure 5: The GUI provides an informative result when using the line thickness calculation app. The user would specify the desired line thickness into the line width field, upon the calculation of the model embedded into the GUI, the pressure, speed, gap, and voltage parameters are determined and can be used in a MEW printer. The live data plot offers a tracking curve to know whether the value is converging to the specified entered line thickness in the calculation part, or it does not. Additionally, the evaluation time helps the end-user to know how much time has elapsed if comparison between model is needed.

Tables

Table 1: Optimized Hyperparameters.

Hyperparameters Name	Search Range	Optimized Hyperparameters
Basis Function	[Constant, Zero, Linear]	Zero
Kernel Function	[Nonisotropic Exponential, Nonisotropic Matern 3/2, Nonisotropic Matern 5/2, Nonisotropic Rational Quadratic, Nonisotropic Squared Exponential, Isotropic Exponential, Isotropic Matern 3/2, Isotropic Matern 5/2, Isotropic Rational Quadratic, Isotropic Squared Exponential]	Nonisotropic Matern 3/2
Kernel Scale	[0.002, 2]	0.53337
Standardize	[True, False]	True
Sigma	[0.0001, 4.6186]	4.5461

Table 2: PID Controllers Values and Back-calculation coefficient.

Parameter	PID Values	Back-calculation coefficient
Gap	[40 30 5]	50
Speed	[0.1 1 0]	-
Voltage	[50 15 1]	40
Pressure	[15 25 1]	-

Table 3: Validation Results obtained by the GUI and custom-designed algorithm.

Desired from GUI	Obtained from Algorithm	Ratio Difference
0.6	1.458559	*2.43093167*
0.4	1.05952	*2.6488*
0.2	0.47128	*2.3564*
1	2.10528	*2.10528*
0.8	1.61336	*2.0167*